Electronic Supplementary Material (ESI) for Nanoscale.

Ultrafast and Broadband Optical Nonlinearity in Aluminum doped Zinc Oxide Colloidal Nanocrystals

Xiangling Tian[a], Hongyu Luo[b], Rongfei Wei[c*], Meng Liu[d], Zhaoliang Yang[e], Zhichao Luo[d], Haiming Zhu[e], Jianfeng Li[b*] and Jianrong Qiu[a,f*]

[a]State Key Laboratory of Luminescent Materials and Devices and School of Materials Science and Engineering, South China University of Technology, Wushan Road 381, Guangzhou 510641, PR China

[b]School of Optoelectronic Science and Engineering, University of Electronic Science and Technology of China, Chengdu, Sichuan, 610054, PR China

[c]Department of Physics, Zhejiang Normal University, Jinhua, Zhejiang, 321004, PR China

[d]School of Information and Optoelectronic Science and Engineering, South China Normal University, Guangzhou, Guangdong 510006, PR China

[e]State Key Laboratory of Chemical Engineering, Center for Chemistry of High-Performance & Novel Materials, Department of Chemistry Zhejiang University, Hangzhou 310027, PR China

[f]State Key Laboratory of Modern Optical Instrumentation, College of Materials Science and Engineering, Zhejiang University, Hangzhou, Zhejiang 310027, PR China

**qjr@zju.edu.cn; rfwei@zjnu.edu.cn; lijianfeng@uestc.edu.cn*

Supporting Information

1. Discussion about response of materials to an optical field.

The light-matter interaction can be described by the material polarization P:[1-4]

$$P = \varepsilon_0 \left[\chi^{(1)} E + \chi^{(2)} E^2 + \chi^{(3)} E^{(3)} + \mathrm{L} \right] \qquad \text{(S1)}$$

here, E usually consists of time-harmonic ω_n, ε_0 and $\chi^{(s)}$ stand for the vacuum permittivity and the sth-order susceptibility of the material, respectively. In weak coupling regime, only the first term ($\chi^{(1)}$) in the equation is efficient, giving rise to a linear response such as refraction, absorption and scattering. However, in the high coupling regime, high orders (s>1) need to be considered. The most important high order terms contain second- ($\chi^{(2)}$) and third-order ($\chi^{(3)}$) interaction. The second-order is usually used to describe second-harmonic generation (SHG), sum- and difference frequency generation, and an electro-optic response, while the third-order interaction contains the Kerr effect, third harmonic generation and four-wave mixing (FWM). Saturable absorption is associated with third-order optical nonlinearities, and can be described by the following equation:[2]

$$\alpha(I) = \frac{\alpha_0}{1 + I / I_s} + \beta I , \qquad \text{(S2)}$$

where I stands for the intensity of incident optical pulse, $\alpha(I)$ presents the intensity-dependent absorption coefficient, α_0 presents the linear absorption coefficient and α_{ns} is non-saturable absorption, respectively. Importantly, the third-order response contains oscillations at the original frequencies, and can result in nonlinear modifications of electronic properties, such as the permittivity and refractive index:[1]

$$\varepsilon = \varepsilon_0 \left[\chi^{(1)} + 3\chi^{(3)} |E|^2 \right] \qquad \text{(S3)}$$

and $n = n_0 + n_2 I$, (S4)

where, ε, ε', ε'', n_0, n_2 and I are the permittivity of materials, the real part, the imaginary part, the linear refractive index, the nonlinear index and the field intensity, respectively.

Owing to the photon-photon interactions enable by materials, optical nonlinearities can be strengthened in material environments that provide mechanisms for field enhancement.[1, 5] Such nonlinear optical effects originate from coherent oscillations of conduction electrons near the surface of nanocrystals when electronic motion in a strong electromagnetic field cannot be considered harmonic. Utilizing the strong electromagnetic field in metal-based plasmonics, both mode-locking and Q-switching pulse can be generated without sacrificing the ultrafast response.[6, 7] However, because of its higher permittivity (*e.g.*, -115 for Ag at 1550 nm), low nonlinearity in infrared (IR) region and the issue of compatibility and integration, advancing these novel optical switches based on metal NCs into practical pulsed lasers is hindered, especially for IR pulsed lasers.[8-10] For

semiconductor nanocrystals, the resonance stems from localized surface plasmons, which can be resonantly excited with light of the appropriate frequency and polarization irrespective of the excitation light wavevector. This can boost nonlinear optical effects in several ways. First, the coupling of light to surface plasmons can result in strong local electromagnetic field, subsequently enhancing optical processes. Second, localized surface plasmons resonance is very sensitive to dielectric properties. As is detected in Fig. 4, the nonlinear refractive index transform from negative value to positive value as the excitation wavelength increases. Third, localized surface plasmons resonance can respond on the timescale of a few femtoseconds, leading to ultrafast response and processing of optical signals.

2. Experimental section.

Synthesis and characterization of AZO NCs

AZO NCs were synthesized in polyol solvent which plays the role of both a complexion agent and a surfactant agent to prevent the agglomeration of the nanoparticles by being absorbed on the nanoparticles surface.[11] Zinc acetate dehydrate (8.714g, $Zn(CH_3COO)\cdot 2H_2O$, 99.99%, Aladdin), aluminum hydroxide (0.193g, $Al(OH)_3$, 99.9%, Aladdin), sodium hydroxide (NaOH, Aladdin) and distilled water (13 ml) were firstly dissolved in 80 ml diethylene glycol (DEG) and then heated up to be 189 ^oC by oil-bath heating. The solution was stirred continuously for 6h by mechanical agitation. Afterward, the solution was cooled down to room temperature to prevent the escape of vapors. The AZO NCs were eventually collected after several operations: centrifuged at 5000 rpm for 5 min to collect the precipitate and then washed 3 times by ethnol; after being centrifuged, the samples were dried in vacuum at 50 ^oC for 12 h. The pure ZnO NCs were also synthesized without adding aluminum hydroxide. Subsequently, the aluminum concentration was measured by ICP-AES to be 2 wt%.

In order to characterize, the sample was prepared by spin-coating the AZO NCs solution (AZO NCs disperse into alcohol by ultrasonic oscillation) onto a 0.5 mm thick high-purity quartz slide for 10 times (also reported in our previous works of *Adv. Mater.* **2017**, *29*, 1700754 and *Adv. Opt. Mater.* **2018**, *6*, 1700948). Raman characterization was measured using a confocal microscopy system (Renishaw inVia, Gloucestershire, UK) operated at 532 nm excitation source at room temperature. A Bruker diffractometer using Cu Kα_1 radiation (λ=1.5418 Å) was employed to determine the crystal phase of the synthesized NCs. The linear optical absorption was performed by a Perkin-Elmer Lambda-900 UV-Vis-NIR spectrophotometer (Perkin Elmer, Waltham, MA). An empty quartz slide was set as a reference. The morphology and crystal structure were recorded by a

transmission electron microscope (TEM, JEOL-2100F) at 200 kV, and dilute solution was dropped onto carbon-coated 200 mesh copper grides to prepare the samples. Elemental analysis was investigated by induced coupled plasma atomic emission spectroscopy (ICP-AES) with a Varian 720/730 Series spectrometer.

Z-scan

Nonlinear optical (NLO) properties of synthesized AZO NCs were performed using a well-developed Z-scan technique. [4, 12] A commercial Ti:sapphire regenerative amplifier system (800 nm, 1 kHz, 120 fs) equipped with an optical parametric amplifier (OPA) was used as the laser source. To detect signal change, InGaAs detectors (Thorlabs, 800-2600 nm) was used. The laser intensity was monitored at the laser foci by a dynamometer. Part of the incident laser beam is separated as a fluctuation reference before the focus lens. The sample (by spin-coating the synthesized NCs onto a 0.5 mm thick high-purity fused quartz slide) was settled on a linear translation stage which can move near the focus to imitate the change of the femtosecond laser intensity. The laser intensity at the focus was monitored to be 1.6 GW cm^{-2} by a dynamometer. An aperture (the smallest size is 1 mm and purchased from Thorlabs) was installed after the samples in order to measure closed- and open-aperture signals. Before operating Z-scan measurement, we employed CS_2 solutions in standard quartz colorimetric utensil to serve as a criterion. Open-aperture signal is normalized by the reference signal and then fitted using equation S9 to obtain nonlinear absorption coefficient β. After dividing the closed-aperture signals by open-aperture measurements, we then fit the results by the equation S11 to calculate nonlinear refractive index n_2.

Pump-probe

For the femtoseconds (fs) transient transmittance spectroscopy, the laser pulses at 1550 nm and 2000 nm with 200 fs pulse duration were generated from a IR OPA (ORPHEUS-ONE, light Conversion Ltd). The output pulses were sent to a delay line as the pump beam to excite the samples. Another 1030 nm femtosecond laser (220 fs Gaussian fit, 100 kHz, Pharos, Light Conversion Ltd) was employed to generate a broadband supercontinuum white light (from 525 nm to 950 nm) to be used as the probe beam by focusing the beam onto a 8 mm YAG plate. The signals were then monitored by a highly sensitive spectrometer (Zolix) with a resolution of 0.5 nm. All the experiments are performed at room temperature. And the samples were prepared by the same process as that of the Z-scan measurement.

3. Calculation of permittivity in aluminum-doped zinc oxide nanocrystals (AZO NCs).

For modeling of AZO NCs, normalized transmittance was used to analytical calculate, as shown in Figure S1. Owing to the diameter is much smaller than the IR wavelength, the average diameter of 25 nm was adopted (determined by TEM in inset in Figure S1). The absorption cross-section of NCs can be written to be:[13]

$$\sigma_{abs} = 4\pi k R^3 \mathrm{Im}\left[\frac{\varepsilon(\omega) - \varepsilon_m}{\varepsilon(\omega) + 2\varepsilon_m}\right], \qquad \text{(S5)}$$

where the NCs radius R is about 12.5 nm, the NCs permittivity is $\varepsilon(\omega)$ and can be described using the equation 1 in the main article and Equation S3. The background permittivity ε_∞ is 4.0,[14] the medium permittivity of quartz slide is 3.78,[15] and the wave vector of light is $k=2\pi/\lambda$. Normalized transmission is calculated by $T=\exp(-\sigma_{abs}NL)$, here N is the NCs concentration on the quartz slide and L=0.5 mm is the thickness of the quartz slide. By fitting the normalized transmittance in Figure S1, we can obtain the related parameters: $\omega_p=2.022\times10^{15}$ Hz, $\gamma=4.308\times10^{14}$ Hz. Therefore, the wavelength-dependent real part and imagine part of permittivity can be obtained through the equation 1 in the main article, as shown in Figure 1d. The carrier density and plasma frequency are followed by:[16] $\omega_p = \sqrt{ne^2/(m_{eff}\varepsilon_0)}$, here n is the electron density, e is the electron charge, ε_0 is the permittivity of free space and m_{eff} presents the electron effective mass, respectively. For AZO, $m_{eff}=0.38m_e$ (m_e is the electron mass).[14] The carrier density is calculated to be about 1.24×10^{19} cm^{-3}, which is smaller than metal-plasmonic materials, leading to the shift of optical response from visible to IR region.[8, 17]

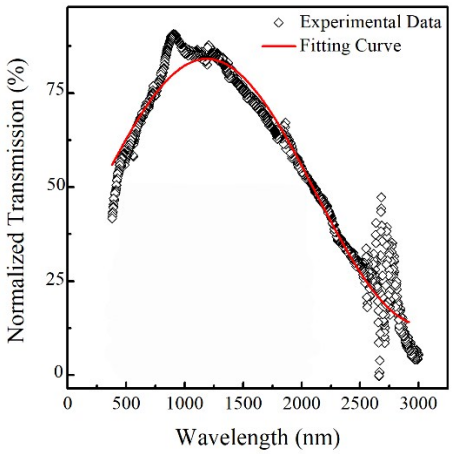

Fig. S1. Experimental transmission spectrum of AZO NCs and a best fit using analytical calculations. The inset are low and high resolution TEM images.

4. Pulse generation

1064 nm fiber laser setup: The laser setup is shown in Fig. S11. The ring cavity configuration is made of all-normal-dispersion fibers, in which a segment of 1 m Yb-doped fiber (YDF) was chosen to be as the gain medium.

A commercial available 980 nm-diode laser with maximum output power of 500 mW was used as pump source to trigger the gain fiber after passing a 980/1060 nm wavelength-division multiplexer (WDM). Two polarization controllers (PCs) were used to adjust the polarization states of the propagation light. The other fibers were HI 1060 fibers with a length of 70.3 m. The cavity roundtrip time was 348.3 ns, corresponding to the total cavity length of 71.3 m. Stable mode-locking operation can be performed by using a bandpass filter centered at 1064 nm with a bandwidth of 5 nm. A polarization-independent isolator (PI-ISO) was used to ensure unidirectional light propagation. A 10% coupler was employed to obtain laser output. To characterize the laser pulse, an optical spectrum analyzer (OSA, Yokogawa AQ6317C) was used to record the output optical spectrum and an oscilloscope (Tektronix DSA-70804, 8GHz) equipped with a 12.5 GHz photodetector (Newport 818-BB-35F) and a radio-frequency (RF) spectral analyzer (Agilent E4407B) was used to analyze the pulses.

1550 nm fiber laser setup: The laser schematic is displayed in Fig. S12. A piece of 4 m erbium-doped fiber (EDF) with a dispersion parameter of -17.3 ps/km/nm was adopted to be as the gain medium. The other fibers were standards single mode fiber (SMF) with a length of 35.5 m. The cavity roundtrip time was 179.86 ns, corresponding to the total cavity length of 39.5 m. An integrated device containing a PI-ISO, WDM and 10% output coupler was used to make the laser cavity more concise, operating to make the pump laser couple into the cavity, ensure unidirectional light propagation and output the laser. A PC was used to adjust the polarization states of the propagation light. The laser performance was simultaneously monitored by an optical spectrum analyzer (OSA, Yokogawa AQ6317C) and a high-speed real-time oscilloscope (Tektronix DSA-70804, 8 GHz) with a photodetector (Newport 818-BB-35F, 12.5 GHz). In addition, an autocorrelator (FR-103XL) was employed to measure the pulse duration.

2000 nm fiber laser setup: The constructed passively Q-switched Tm-doped fiber (TDF) laser cavity are based on AZO NCs saturable absorber. The pump source was a commercial 793 nm laser diode (LD) (BWT, Beijing) with a multimode fiber pigtail which has a 105 μm core diameter and a numerical aperture (NA) of 0.22. The pump laser was launched into the gain fiber through a (2+1)×1 combiner (IFT, Canada). The gain fiber was a piece of 2.0 m double-cladding TDF (Coractive, DCF-TM-10/128) with an octagonal shaped inner cladding with a diameter of 128 μm and a NA of 0.45, and a circular core with a diameter of 10 μm diameter and a NA of 0.22. The cladding absorption coefficient of ~4 dB/m measured at 793 nm gave a nominally 94% total absorption at this length. A 50:50 coupler (IFT, Canada) was spliced with the TDF to output half of the signal laser. PI-ISO

was to maintain the intra-cavity laser propagate unidirectionally. The AZO/poly(vinyl alcohol) (PVA) film sandwiched between two FC/PC connectors was connected with a flange as the saturable absorber device. A PC was placed between the combiner and saturable absorber device to control the intra-cavity loss. When the intensity of the propagation light in the fiber waveguide is large enough for the AZO film to trigger a Q-switching operation, stable Q-switching regime with a low amplitude fluctuation of ±3% was obtained. The temporal pulse train and single pulse waveforms were monitored using a InGaAs photodetector (EOT ET-5000F, USA) equipped with an 8 GHz digital oscilloscope. The radio frequency (RF) spectrum was performed by a RF spectrum analyzer (YIAI, China, AV4033A, 30Hz-18GHz). The optical spectrum was investigated using an optical spectrum analyzer (Yokogawa AQ6375, Japan) with a resolution of 0.05 nm. The output power was recorded using a thermal power sensor (S470C, Thorlabs, USA).

3000 nm fiber laser setup: The schematic of the pulsed fiber laser can be found in our previous work.[12, 18] In short, two commercially available diode lasers (1150 nm, Eagleyard Photonics, Berlin) was employed as pump source to trigger the gain fiber (commercial double-cladding Ho^{3+}/Pr^{3+}-codoped ZBLAN fiber with the concentration of Ho^{3+}-30000 and Pr^{3+}-2500 ppm, fiberlabs, Japan). The gain fiber had an octangular pump core with a diameter of 125 μm and a NA of 0.5, and a circular core with a diameter of 125 μm and a NA of 0.2. The laser was firstly collimated by an uncoated ZnSe objective lens (focal length: 6 mm, Innovation Photonics, LFO-5-6, 0.25 NA) and then focused by another same ZnSe objective lens terminated with the AZO/PVA composite film (coated commercial gold-protected mirror). An InAs detector with a response time of 2 ns equipped with a 500 MHz bandwidth digital oscilloscope was employed to record temporal pulse trains and waveforms. The RF spectrum was performed using a RF spectrum analyzer (AV4033A) with a scanning range of 30 Hz-18 GHz. A monochromator with a scanning resolution of 0.1 nm (Princeton instrument Acton SP2300) was used to identify the optical spectrum.

Nonlinear absorption (NLA) measurement

NLA measurement at 1550 nm: Fig. S8 displays the schematic used for nonlinear absorption measurement of AZO/PVA composite film at 1550 nm. The composite film was used as same as that in laser cavity for pulsed laser generation. The pump source was an in-house made femtosecond pulse pump source with the center wavelength of 1554.4 nm, a repetition rate of 26 MHz and a pulse duration of 500 fs. The output femtosecond pulse from the fiber laser is amplified by a commercial erbium-doped fiber amplifier (EDFA) to increase the

output power. The input optical power was controlled by a variable optical attenuator. The output laser was split into two parts using a 50:50 coupler, one of which was used as the reference while another part was connected with saturable absorber. A powermeter was employed to monitor the output laser.

NLA measurement at 2000 nm: The inset in Fig. S9 shows the schematic of arrangement used for nonlinear absorption measurement of AZO/PVA composite film at 2000 nm. The laser source was an in-house ultrashort pulse fiber laser system including a nonlinear polarization rotation (NPR) mode-locked TDF laser seed followed by a TDF fiber based amplifier. It has a center wavelength of 1980 nm, a repetition rate of 30.4 MHz and a pulse width of 1.25 ps. The output laser was split into two channels using a 10:90 coupler. The 10% port was directly monitored by a detector of a powermeter as the reference. The 90% port was connected with the AZO/PVA composite film (saturable absorber) as same as the one used in the laser cavity. Then the output laser from the SA device was monitored by another detector of the powermeter. Note that the insertion loss introduced by two FC/PC connectors have been removed when calculating the nonlinear absorption.

NLA measurement at 3000 nm: A typical power dependent measurement setup was built up to reveal the nonlinear absorption of AZO NCs, as shown in Fig. S10. The pump source was a self-built SESAM passively mode-locked Ho^{3+}/Pr^{3+} co-doped ZBLAN fiber laser with an output laser centered at 2868.0 nm (pulse duration: 20 ps, repetition rate: 17.86 MHz). A beam splitter with transmittance/reflectance ration of 55:45 was employed to split the laser into two parts. The reflectance laser was focused by an uncoated CaF_2 lens (focal length: 20 mm, LA5315, Thorlabs) and then went through a CaF_2 substrate to serve as the reference. The transmittance laser was focused by another same CaF_2 lens and then went through a CaF_2 substrate coated with AZO NCs. Two powermeters were used to detect the output power.

4. Calculation of nonlinear absorption coefficient

According to NLO theory, the propagation can be described:[2]

$$\frac{\mathrm{d}I}{\mathrm{d}z'} = -\alpha(I)I, \qquad \text{(S6)}$$

here, z' present the propagation length in the samples, I is the incident intensity of laser. The total absorption $\alpha(I)$ contains two parts: a linear absorption coefficient α_0 and a nonlinear absorption coefficient α_{NL}. Therefore, the total absorption can be:

$$\alpha(I) = \alpha_0 + \alpha_{NL}I. \qquad \text{(S7)}$$

For a system, we can also describe $\alpha(I)$ using the following relationship:

$$\alpha(I) = \frac{\alpha_0}{1 + I/I_s} + \beta I , \qquad \text{(S8)}$$

where β is nonlinear absorption coefficient. Hence, the normalized transmittance can be described by:

$$T = \frac{1}{\sqrt{\pi}\left[\frac{\beta I_0 L_{eff}}{\left(1+z^2/z_0^2\right)}\right]} \int_{-\infty}^{+\infty} \times \ln\left[1 + \frac{\beta I_0 L_{eff}}{\left(1+z^2/z_0^2\right)} \exp\left(-t^2\right)\right] dt . \qquad \text{(S9)}$$

Here T, I_0, and L are the normalized transmittance, the peak light intensity at the focus, the thickness of the AZO film and the diffraction length of the beam, respectively. The effective length of the sample, L_{eff}, can be defined as: $L_{eff} = \left(1 - e^{-\alpha_0 L}\right)/\alpha_0$. z_0 stands for the diffraction length of the beam: $z_0 = \pi\omega_0^2/\lambda$, with ω_0 is the beam waist radius.

The imaginary part of the third-order nonlinear susceptibility can be expressed:

$$\mathrm{Im}\chi^{(3)}(\mathrm{esu}) = \frac{10^{-7} c^2 n_0^2}{96\pi^2 \omega}\beta . \qquad \text{(S10)}$$

Where, c, λ, and n are, respectively, the speed of light in the vacuum, the wavelength of incident light, and the refractive index.

From the division of the closed-aperture Z-scan by the corresponding OA result, the NLO refractive index n_2 can be extracted from the fitting curve by the following formula:

$$T = 1 + \frac{4x\Delta\Phi}{\left(1+x^2\right)\left(9+x^2\right)} + \frac{4\left(3x^2-5\right)\Delta\Phi^2}{\left(1+x^2\right)^2\left(9+x^2\right)\left(25+x^2\right)} + \frac{32\left(3x^2-11\right)x\Delta\Phi^3}{\left(1+x^2\right)^3\left(9+x^2\right)\left(25+x^2\right)\left(49+x^2\right)} \qquad \text{(S11).}$$

Where, the on-axis nonlinear phase shift at the focus is $\Delta\Phi = kI_0(n_2 L_{\text{eff}} + n_{2-\text{quartz}} L_{\text{quartz}})$, here, n_2 describes nonlinear refractive index of materials and $n_{2\text{-quartz}}$ describes nonlinear refractive index of fused quartz substrate, which is about 2.0×10^{-7} cm^2 GW^{-1};[19] L_{quartz} is the thick of fused silca. k is the wavelength number; $x=Z/Z_0$. Therefore the real part of the third-order nonlinear susceptibility can be extracted from the following relation

The figure of merit (FOM) is calculated as:

$$\mathrm{FOM} = \left|\frac{\mathrm{Im}\chi^{(3)}}{\alpha_0}\right| . \qquad \text{(S12)}$$

Additional Figures

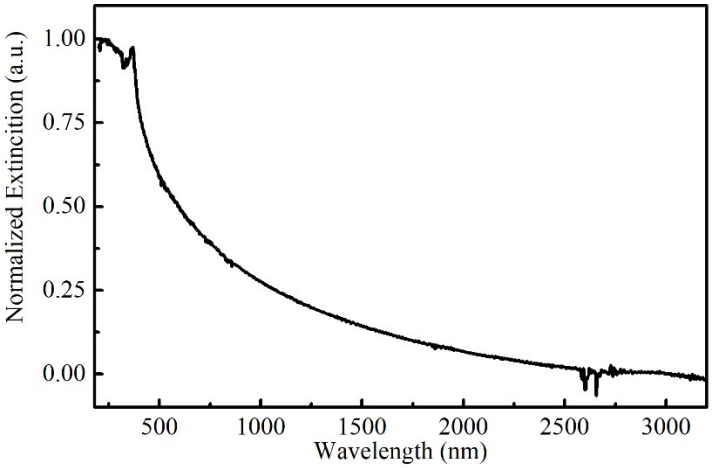

Fig. S2. Normalized extinction spectrum of ZnO NCs.

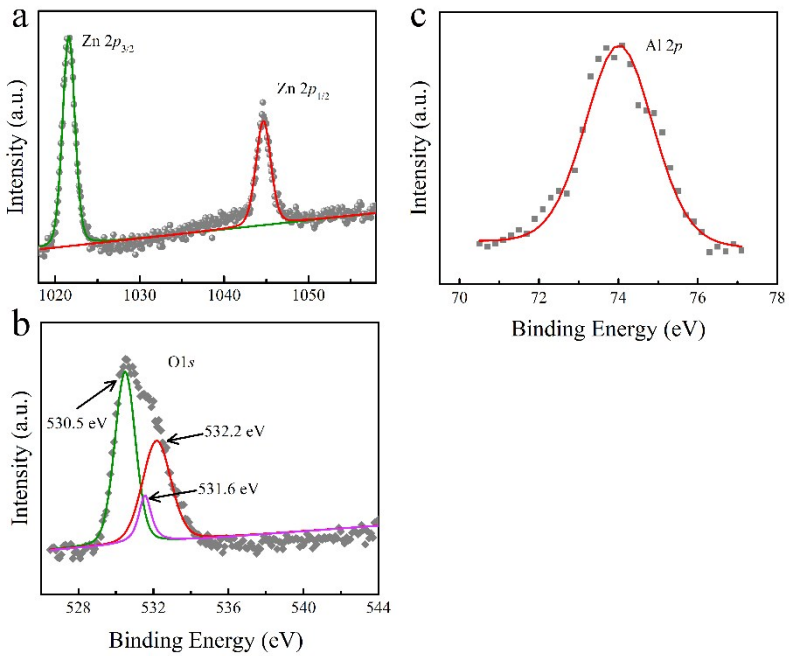

Fig. S3. XPS characterization of Zn2*p* (a), O1*s* (b) and Al2*p* (c) for AZO NCs. The binding energy of the Zn2$p_{3/2}$ locates at 1021.7 eV, which is larger than that in ZnO. The O1*s* peak can be fitted by three components, which locate at 530.5 eV, 531.6 eV, and 532.2 eV, respectively. The binding energy of the Al2*p* locates at 73.9 eV, indicative of a characteristic of Al_2O_3. Noteworthy, no peak at 72.7 eV are detected, indicating nonexistence of metallic aluminum.[20]

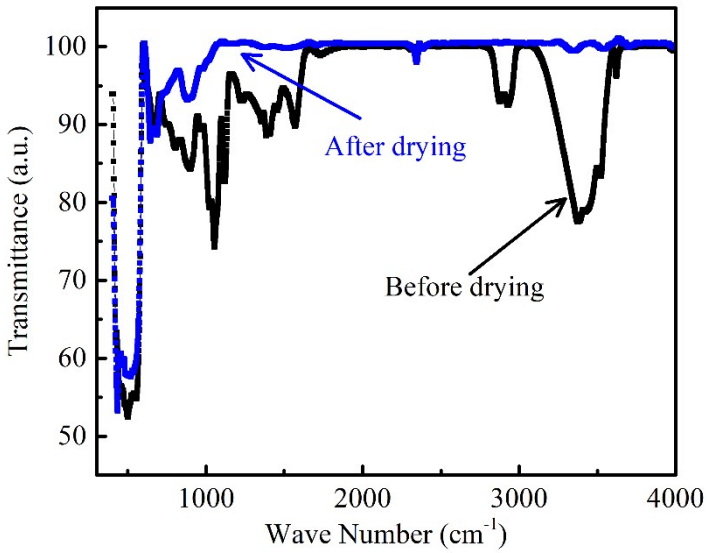

Fig. S4. Fourier transform infrared (FTIR) spectra of AZO NCs before and after drying in vacuum. Clearly, the O-H vibration, C-H modes, C-O and C-C centered at 3450 cm^{-1}, 2855 cm^{-1}, 2925 cm^{-1}, 1624 cm^{-1} and 1385 cm^{-1} disappears after drying in vacuum.[21] The strong absorption at about 460 cm^{-1} stems from the stretching vibration of ZnO bond.[21] The addition absorption band between 4000 and 1500 cm^{-1} originates from surface plasmon absorption and the presence of free charge carriers.[22]

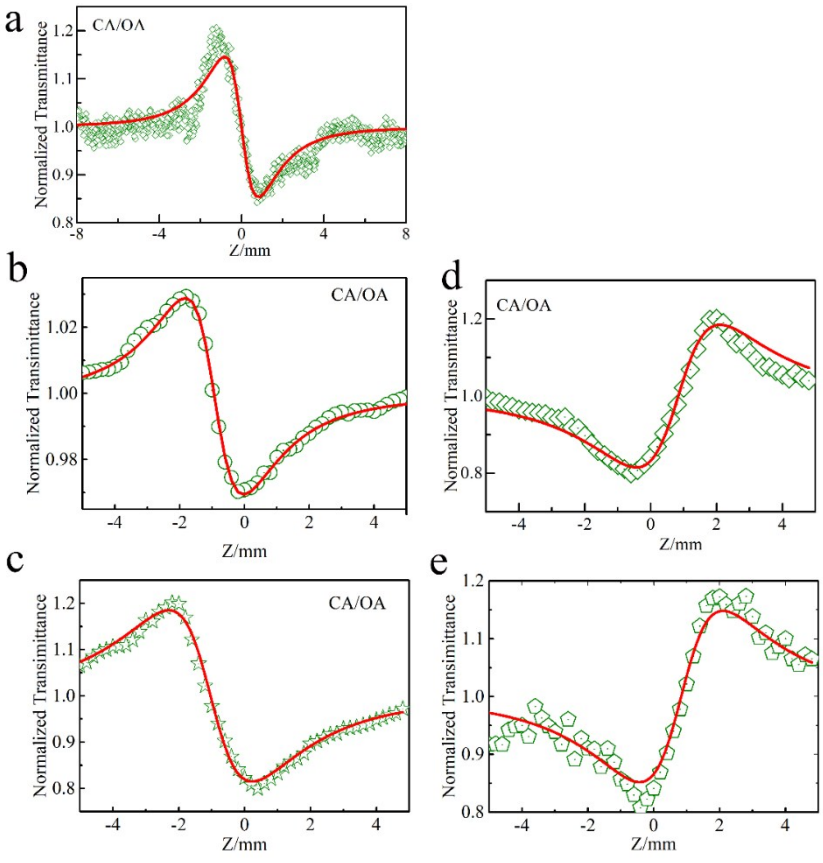

Fig. S5. Nonlinear optical properties of obtained AZO NCs. CA/OA curves under different excitation wavelength: (a) 800 nm, (b) 1064 nm, (c) 1550 nm, (d) 2000 nm and (e) 2550 nm. All the measurements are recorded at room temperature.

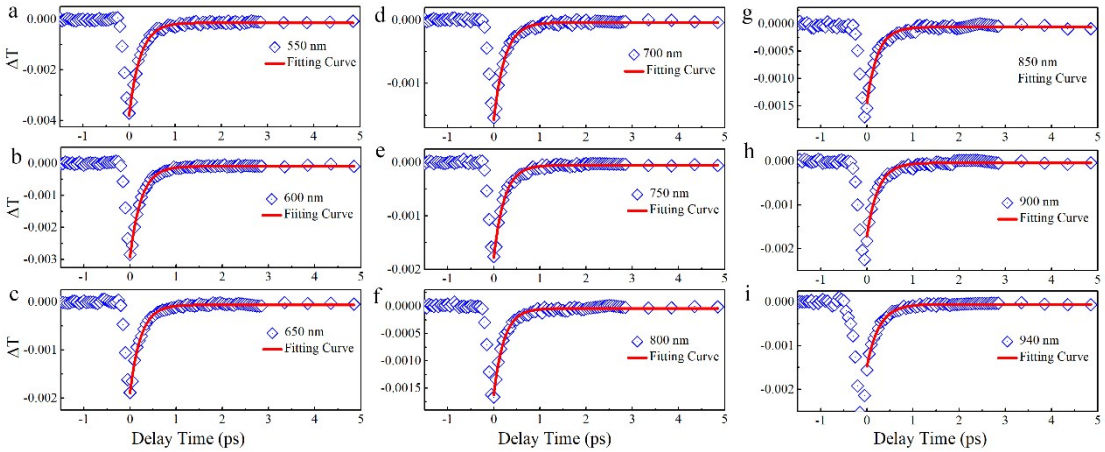

Fig. S6. Measured transitivity transients of AZO with different probe wavelength from 550 nm to 940 nm are extracted from Fig. 3a in main text (pump wavelength: 1550 nm). The squares present experimental data and the red line is fitting curves using a single-exponential model.

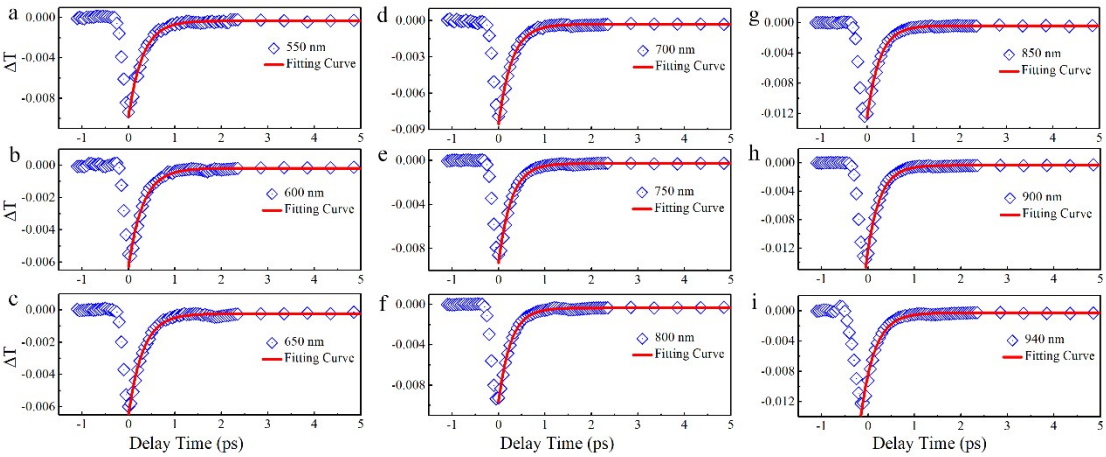

Fig. S7. Measured transitivity transients of AZO with different probe wavelength from 550 nm to 940 nm are extracted from Fig. 3c in main text (pump wavelength: 2000 nm). The squares present experimental data and the red line is fitting curves using a single-exponential model.

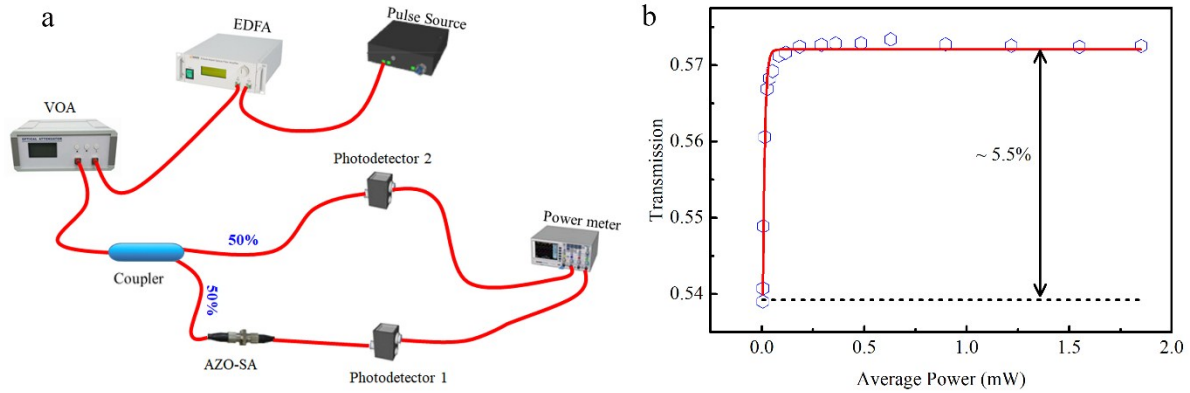

Fig. S8. (a) Experimental setup of nonlinear absorption measurement at 1533.8 nm. (b) Transmittance as a function of pulse peak intensity. The extracted saturable intensity and nonsaturable absorption are 0.001 mW and 42.6 %, respectively.

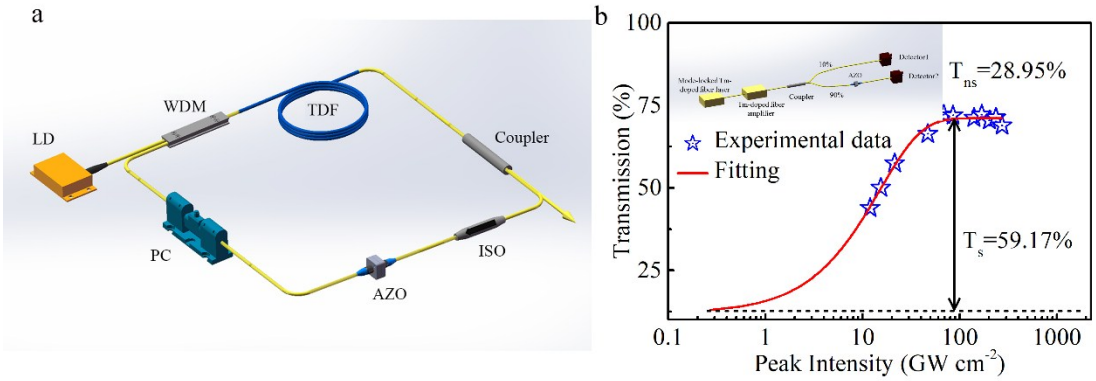

Fig. S9. (a) Schematic illustration of a passively Q-switched Tm-doped fiber laser constructing a ring cavity using AZO as absorber. (b) Nonlinear transmittance as a function of pulse peak intensity at 1960.3 nm. The inset is experimental setup of nonlinear absorption measurement. The extracted saturable intensity and nonsaturable absorption are 15.05 GW cm^{-2} and 28.95 %, respectively.

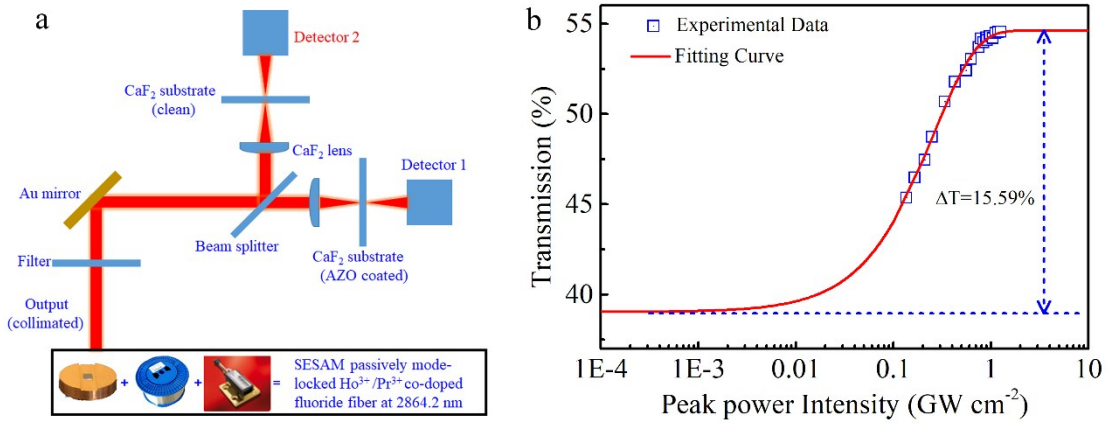

Fig. S10. (a) Experimental setup of nonlinear absorption measurement at 2864.2 nm. (b) Nonlinear transmittance as a function of pulse peak intensity at 2864.2 nm. The extracted saturable intensity and nonsaturable absorption are 0.26 GW cm^{-2} and 45.3 %, respectively.

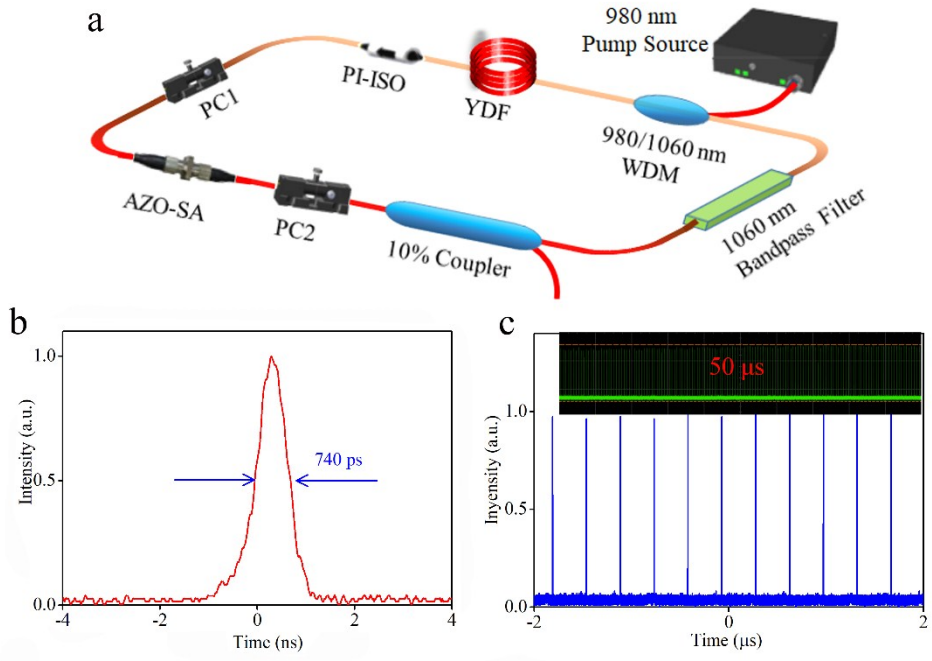

Fig. S11. Mode-locking operation in YDF laser based on ultrafast all-optical switch of AZO. (a) Schematic illustration of a passively mode-locked laser constructing a ring cavity. (b) Pulse duration of single pulse. (c) Typical laser output pulse train.

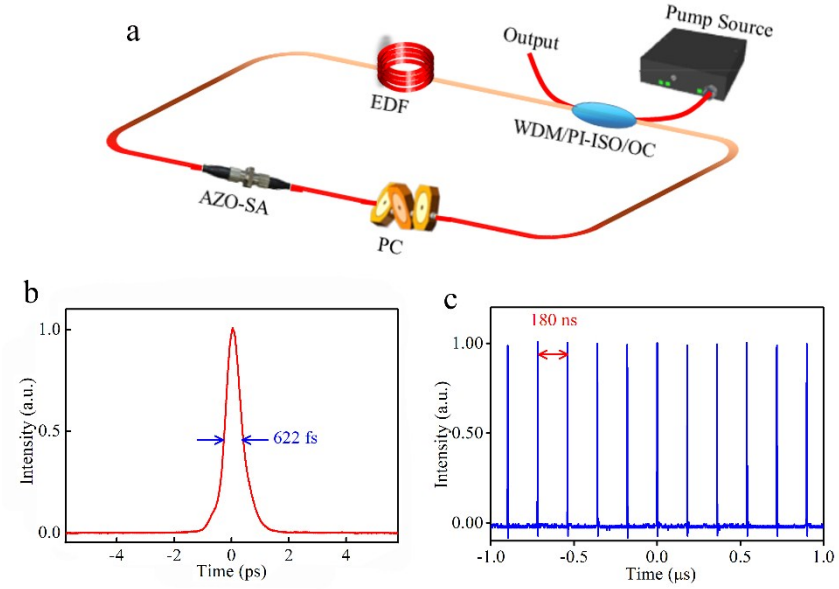

Fig. S12. Mode-locking operation in EDF laser based on ultrafast all-optical switch of AZO. (a) Schematic illustration of a passively mode-locked laser constructing a ring cavity. (b) Autocorrelation trace. (c) Typical laser output pulse train.

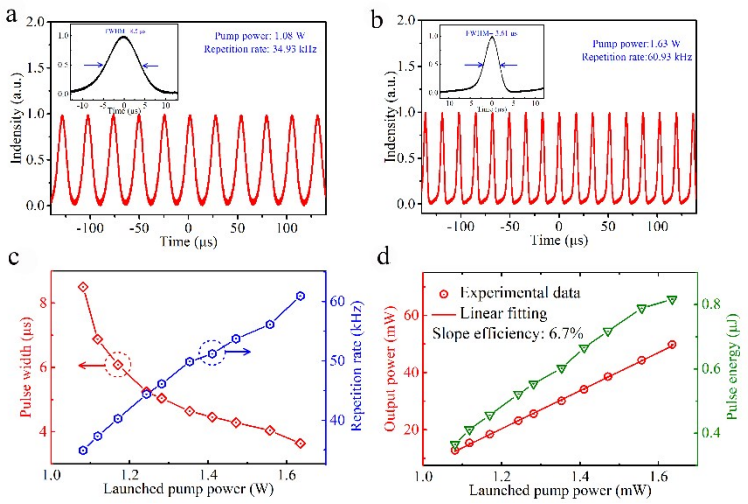

Fig. S13. Q-switching characterization of AZO switch-based TDF laser. Typical Q-switched pulses trains at the pump power of (a) 1.08 W and (b) 1.63 W. The inset is single pulse envelope. (c) The pulse duration and the pulse repetition rate as a function of incident pump power. (d) The output power (triangle) and the pulse energy (circle) as a function of incident pump power.

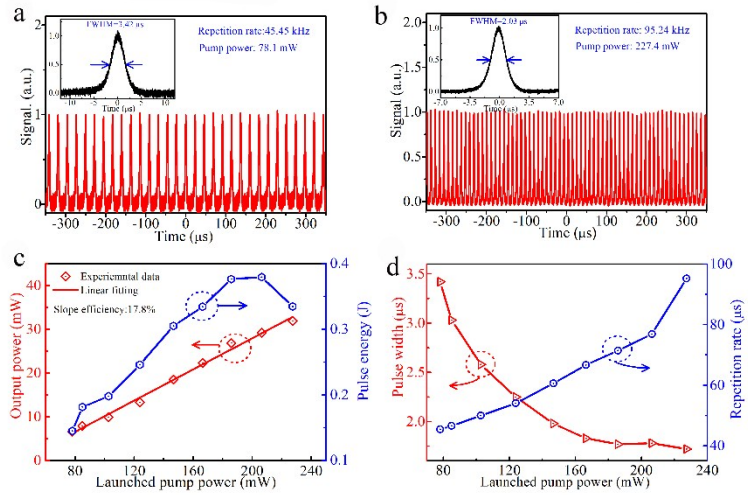

Fig. S14. Q-switching characterization of AZO switch-based Ho/Pr co-doped ZBLAN fiber laser. Typical Q-switched pulses trains at the pump power of (a) 78.1 mW and (b) 227.4 mW. The inset is single pulse envelope. (c) The pulse duration and the pulse repetition rate as a function of incident pump power. (d) The output power and the pulse energy as a function of incident pump power.

Additional Tables

Table S1 NLO parameters of several typical materials

Laser	Sample	β (cm GW^{-1})	Im $\chi^{(3)}$ (esu)	FOM (esu cm)
1030 nm, 1kHz, 340 fs	MoS_2 [23]	-(9.17±2.56)×10^{-2}	-(6.7±1.9)×10^{-14}	(5.7±1.6)×10^{-15}
	$MoSe_2$ [20]	-(1.29±0.13)×10^{-2}	-(9.4±1.0)×10^{-15}	(4.22±0.27)×10^{-15}
	$MoTe_2$ [20]	-(7.50±0.47)×10^{-3}	-(5.50±0.34)×10^{-15}	(6.38±0.39)×10^{-15}
	Graphene [20]	-(9.40±3.18)×10^{-2}	-(6.9±2.3)×10^{-14}	(4.03±1.36)×10^{-15}
800 nm, 1 kHz, 100fs	MoS_2 [20]	-(2.42±0.80)×10^{-2}	-(1.38±0.45)×10^{-14}	(1.23±0.40)×10^{-15}
	$MoSe_2$ [20]	-(2.54±0.60)×10^{-3}	-(1.45±0.34)×10^{-15}	(6.9±1.6)×10^{-16}
	$MoTe_2$ [20]	-(3.7±1.2)×10^{-3}	-(2.13±0.66)×10^{-15}	(1.45±0.45)×10^{-15}
	Graphene [20]	-(1.52±0.42)×10^{-2}	-(8.7±2.4)×10^{-15}	(4.9±1.4)×10^{-16}
1550nm, 35fs	Black Phosphor-us[24]	-0.15×10^{-3}	N/A	N/A
800 nm, 1kHz, 100 fs	Black Phosphor-us[25]	-(4.08±0.11)×10^{-3}	N/A	N/A
1550 nm, 150 fs	SWNTs[26]	N/A	10^{-10}	N/A
800 nm, 220 fs	Au nanorodes[27]	-1.5	-1.2×10^{-12}	3×10^{-14}
800 nm, 120 fs	AZO NCs [a]	-6.04×10^2	N/A	N/A
1064 nm, 120 fs	AZO NCs [a]	-1.02×10^3	N/A	N/A
1550 nm 120 fs	AZO NCs [a]	-1.90×10^3	N/A	N/A
2000 nm 120 fs	AZO NCs [a]	--1.79×10^3	N/A	N/A

[a]This work

References:

1. M. Kauranen and A. V. Zayats, *Nat. Photonics*, 2012, **6**, 737.
2. T. Hasan, Z. Sun, F. Wang, F. Bonaccorso, P. H. Tan, A. G. Rozhin and A. C. Ferrari, *Adv. Mater.*, 2009, **21**, 3874-3899.
3. S. Wang, H. Yu, H. Zhang, A. Wang, M. Zhao, Y. Chen, L. Mei and J. Wang, *Adv. Mater.*, 2014, **26**, 3538-3544.
4. X. Tian, R. Wei, M. Liu, C. Zhu, Z. Luo, F. Wang and J. Qiu, *Nanoscale*, 2018, **10**, 9608-9615.
5. G. X. Ni, L. Wang, M. D. Goldflam, M. Wagner, Z. Fei, A. S. McLeod, M. K. Liu, F. Keilmann, B. Özyilmaz, A. H. Castro Neto, J. Hone, M. M. Fogler and D. N. Basov, *Nat. Photonics*, 2016, **10**, 244.
6. Z. Liu, H. Mu, S. Xiao, R. Wang, Z. Wang, W. Wang, Y. Wang, X. Zhu, K. Lu, H. Zhang, S.-T. Lee, Q. Bao and W. Ma, *Adv. Mater.*, 2016, **28**, 3535-3542.
7. Z. Kang, Y. Xu, L. Zhang, Z. Jia, L. Liu, D. Zhao, Y. Feng, G. Qin and W. Qin, *Appl. Phys. Lett.*, 2013, **103**, 041105.
8. G. V. Naik, J. Liu, A. V. Kildishev, V. M. Shalaev and A. Boltasseva, *Proc. Natl. Acad. Sci. USA*, 2012, **109**, 8834-8838.
9. I. Liberal and N. Engheta, *Nat. Photonics*, 2017, **11**, 149.
10. M. Z. Alam, I. De Leon and R. W. Boyd, *Science*, 2016, **352**, 795.
11. M. Louhichi, S. Romdhane, A. Fkiri, L. S. Smiri and H. Bouchriha, *Appl. Surf. Sci.*, 2015, **356**, 998-1004.
12. X. Tian, H. Luo, R. Wei, C. Zhu, Q. Guo, D. Yang, F. Wang, J. Li and J. Qiu, *Adv. Mater.*, 2018, **30**, 1801021.
13. B. T. Diroll, P. Guo, R. P. H. Chang and R. D. Schaller, *ACS Nano*, 2016, **10**, 10099-10105.
14. A. V. Singh, R. M. Mehra, N. Buthrath, A. Wakahara and A. Yoshida, *J. Appl. Phys.*, 2001, **90**, 5661-5665.
15. D. K. Ghodgaonkar, V. V. Varadan and V. K. Varadan, *IEEE T. Instrum. Meas.*, 1990, **39**, 387-394.
16. Y. Yang, K. Kelley, E. Sachet, S. Campione, T. S. Luk, J.-P. Maria, M. B. Sinclair and I. Brener, *Nat. Photonics*, 2017, **11**, 390.
17. A. Boltasseva and H. A. Atwater, *Science*, 2011, **331**, 290-291.
18. H. Luo, X. Tian, Y. Gao, R. Wei, J. Li, J. Qiu and Y. Liu, *Photonics Res.*, 2018, **6**, 900-907.
19. D. Milam, *Appl. Opt.*, 1998, **37**, 546-550.

20. L. Li, L. Fang, X. J. Zhou, Z. Y. Liu, L. Zhao and S. Jiang, *J. Electron Spectrosc.*, 2009, **173**, 7-11.
21. R. Buonsanti, A. Llordes, S. Aloni, B. A. Helms and D. J. Milliron, *Nano Lett.*, 2011, **11**, 4706-4710.
22. Z. Lu, J. Zhou, A. Wang, N. Wang and X. Yang, *J. Mater. Chem.*, 2011, **21**, 4161-4167.
23. K. Wang, Y. Feng, C. Chang, J. Zhan, C. Wang, Q. Zhao, J. N. Coleman, L. Zhang, W. J. Blau and J. Wang, *Nanoscale*, 2014, **6**, 10530-10535.
24. Y. Wang, G. Huang, H. Mu, S. Lin, J. Chen, S. Xiao, Q. Bao and J. He, *Appl. Phys. Lett.*, 2015, **107**, 091905.
25. S. B. Lu, L. L. Miao, Z. N. Guo, X. Qi, C. J. Zhao, H. Zhang, S. C. Wen, D. Y. Tang and D. Y. Fan, *Opt. Express*, 2015, **23**, 11183-11194.
26. Y.-C. Chen, N. R. Raravikar, L. S. Schadler, P. M. Ajayan, Y.-P. Zhao, T.-M. Lu, G.-C. Wang and X.-C. Zhang, *Appl. Phys. Lett.*, 2002, **81**, 975-977.
27. H. I. Elim, J. Yang, J.-Y. Lee, J. Mi and W. Ji, *Appl. Phys. Lett.*, 2006, **88**, 083107.